ARTICLE IN PRESS
+ MODEL
Frontiers of Architectural Research xxx (xxxx) xxx

Higher Education Press

Available online at www.sciencedirect.com
ScienceDirect
journal homepage: www.keaipublishing.com/foar

SOUTHEAST UNIVERSITY

RESEARCH ARTICLE

3D extrusion of multi-biomaterial lattices using an environmentally informed workflow

Vasiliki Panagiotidou, Andreas Koerner, Marcos Cruz, Brenda Parker*, Bastian Beyer, Sofoklis Giannakopoulos

Bio-Integrated Design Lab, The Bartlett School of Architecture, University College London, London, WC1E 6BT, United Kingdom

Received 6 December 2021; received in revised form 19 June 2022; accepted 20 June 2022

KEYWORDS
Hydrogels;
Multi-biomaterials;
Hygroscopic properties;
Pneumatic extrusion;
Environmentally informed deposition;
Integrated workflows

Abstract The conventional building material palette has been proven limited in terms of adaptability to our current environmental challenges. Innovations in computational design and digital manufacturing have supported the broadening of biomaterial applications as an alternative. While biomaterials are characteristically responsive to stimuli such as temperature and humidity, their unpredictable behaviour is a hurdle to standardization and architectural utilisation. To examine the nexus between material formulation, computation and manufacturing, multi-biomaterial lattice structures were produced through an environmentally informed workflow. Customized biomaterial development resulted in three candidate biopolymer blends with varying levels of hydro-responsiveness and transparency. The computational strategy included a machine learning clustering algorithm to customise results and dictate material distribution outputs. To test the workflow, environmental data of solar radiation exposure and solar heat gain from a specific location was used to inform the material deposition via pneumatic extrusion for the design and digital fabrication of a deformation-controlled prototype of 350 mm × 350 mm. This led to a series of multi-biomaterial wall panel components that can be applied at architectural scale. In future, these techniques can support the incorporation of living elements to be embedded within the built environment for truly animate architecture.

* Corresponding author.
E-mail address: brenda.parker@ucl.ac.uk (B. Parker).
Peer review under responsibility of Southeast University.

https://doi.org/10.1016/j.foar.2022.06.010

Please cite this article as: V. Panagiotidou, A. Koerner, M. Cruz et al., 3D extrusion of multi-biomaterial lattices using an environmentally informed workflow, Frontiers of Architectural Research, https://doi.org/10.1016/j.foar.2022.06.010

1. Introduction

Anthropogenic climate change has highlighted the limitations of our conventional building materials concerning their adaptability to environmental conditions. According to The Royal Society (2021) in recent decades this led to a series of innovations to develop more responsive elements for architecture. Amongst these, biomaterials offer many interesting properties and a potentially more sustainable methods of manufacture. By combining multiple different biocomposites, the outputs can be tuned, or functionalities added. Here, the focus is on multi-biomaterial composites in conjunction with computational design and CNC-extrusion as a means to realise versatile structures.

1.1. Biomaterials

Biomaterials as a term define any kind of natural or synthetic matter, surface, or construct with the capacity to interact with biological systems (NIBIB, 2021). Hydrogels are a specific subcategory, as polymer-based hydrophilic structures that create the necessary conditions of water availability to support cellular life. They are materials of high interest due to their capacity to support cell growth for a range of applications (Tsou et al., 2016; Bae et al., 2015). In particular, algae-laden hydrogels may enable functionality, such as carbon dioxide sequestration (Sayre, 2010) and bioremediation of organic pollutants (Ben Chekroun et al., 2014). A wide range of stimuli-responsive hydrogels have also been developed over the past decades. The material responsiveness refers to their dynamic properties, triggered by external factors like temperature, pH, light, magnetic and electrical fields, shear forces, and chemicals, leading to changes in swelling, porosity, physical structure, and modulus (Chatterjee and Chi-leung Hui, 2018). Responsive hydrogels have become of interest to design-related fields, as means of expanding current material options and the potential to become animate through their physical behaviour and capacity to support biological growth (The Royal Society, 2021). Animate materials have been defined as being sensitive to their environment due to their capacity to adjust and fulfil their function, using behaviours that may be active, adaptive, and/or autonomous. In the context of bio-integrated design, they may be either biohybrid structures that encapsulate cells within non-living matrices, adding a geometric dimension to immobilisation, or engineered living materials (ELMs) that are composed of living cells capable of modulating the functional performance of the grown composite itself. When employed within the built environment, the unique properties of these materials offer the potential to enhance the spatial experience and architectural quality. Installations such as *Aguahoja* by Mediated Matter Group (Tai et al., 2018) make use of multimateriality with bio-based materials. Going further, multi-biomateriality offers the potential to embed living cells within biocompatible materials fabricated using advanced manufacturing techniques as a means of creating three-dimensional animate structures. The rapid expansion of the biomaterial palette also led to innovation in existing fabrication methods (Min et al., 2015). Three-dimensional extrusion-based bioprinting is an emergent technique, which combines biomaterials and fabrication. It allows the prototyping of structures able to display specific biological functions (Chua and Yeong, 2015), such as customised cell immobilisation (Malik et al., 2020), or material-driven chemical signalling (Smith et al., 2019). However, they are challenging materials for precise extrusion-based fabrication due to a lack of strength and control of mechanical properties (Kim et al., 2019), which limits the existing options of printable hydrogel systems (Li et al., 2020). Also, compared to conventional building materials in architecture, hydrogels have a significantly shorter life cycle, requiring their fabrication process to be repeated every few months (Tai et al., 2018). As a result, hydrogels are fitting candidates for agile applications, such as the scaffold for living elements that require frequent replacement.

1.2. Gradience

It has been identified that the greatest challenges underlying the application of biomaterials are scalability, replicability and standardised control when challenged with the utilisation of CAD and CAM technologies combined with high-resolution automated additive manufacturing methods (Smith et al., 2019). Novel materials but also new ways of articulation have recently been at the forefront of research for architecture and construction (Hensel and Menges, 2006). In nature, biological structures display intricate volumetric variance and complexity, that allows for permeability, interconnections and inseparable integration of individual parts. However, in comparison to biological structures, the outputs of standardised articulation of discrete homogenous elements display deficiencies on a functional and variational level (Duro-Royo et al., 2015). Computational tools and 3D printing allow us to break this standardization and to customise not just on a macro, but also on a micro-scale (Carpo, 2016). In addition to adaptive design customisation, digital fabrication can also optimise material usage and help balance environmental impacts in architecture (Kreysler, 2010). Nonetheless, the application of functionally graded materials (FGM) remains limited by computational design and digital fabrication constraints (Duro-Royo et al., 2015). Gradient generation in the field of bioprinting remains primarily a result of structural, chemical or formal differentiation. Within the area of FGM structural or shape optimization and are mainly focused on stiffness gradients, where form and shape are the determining factors of gradience across the structure (An et al., 2015). Smart hydrogels combined with methods of characterisation and modelling can unveil new application possibilities for these materials (Wang et al., 2015). Moreover, existing approaches of gradient generation are single-cycle processes, initiated by invasive methods such as insertion of chemicals, presence of substances, specific temperature, light or pH conditions. Alternatively, this may be through top-down actions like a multimaterial deposition.

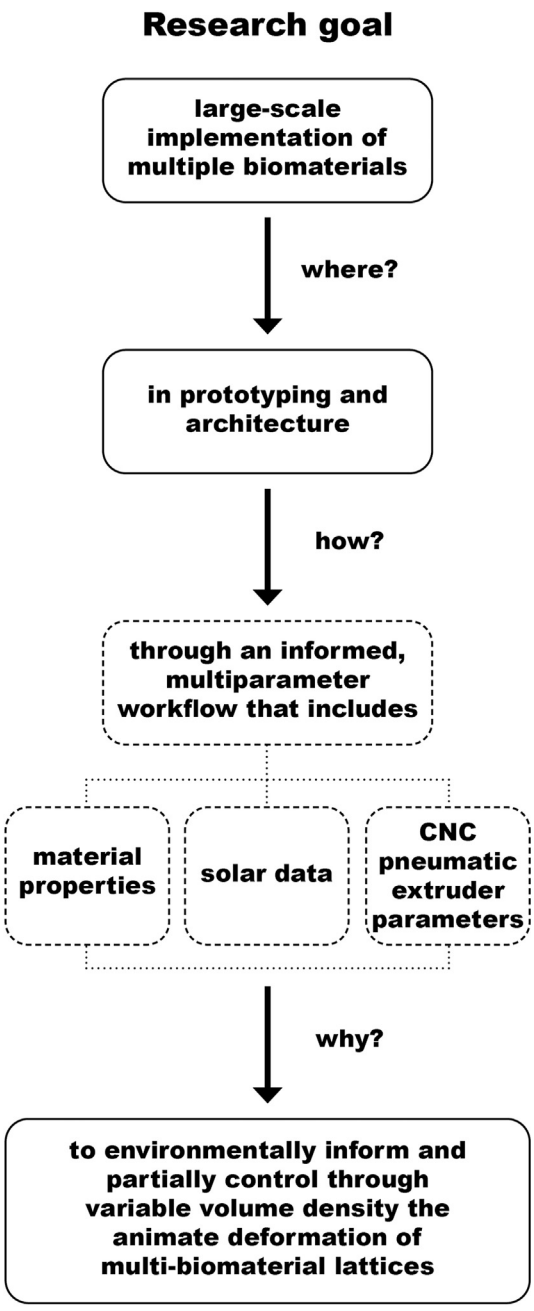

Fig. 1 Overview of research design.

1.3. Environmentally informed design and fabrication

In digital architectural design, environmental simulations are now used to articulate and depict environmental processes (Peters, 2018), or to predict and evaluate future performances (Peters and Peters, 2017). The term "environment" in this context refers to three types of conditions which play a critical role in the research development. The first relates to the variability of the overall environmental context, which includes both outdoor and indoor conditions. The second and third is the sensitivity of biomaterials to fluctuations in such ambient, and how the fabrication process may be impacted by these interactions with manufacturing techniques. In large-scale additive manufacturing of biomaterials, noteworthy challenges appear (Mogas-Soldevila et al., 2014) mostly related to the predictability and the repeatability of hydrogel behaviour, which is dependent on the interplay between fabrication and material composition factors (Malik et al., 2020). For future building applications, a more efficient workflow that unifies the design, material/fabrication and environmental context is needed for the realisation of multi-biomaterial structures (Duro-Royo et al., 2015). In the case of hygroscopic, water-based biomaterials, defining the parameters that drive the material differentiation and performance is of critical importance both on a morphological and structural level. A demonstration of a controlled performance in this context refers to the hypothesis that the varying volume density in the multi-biomaterial deposition results in its guided deformation from a flat extruded lattice to a curved one upon drying.

To evaluate the level of predictive control that could be exerted in a multi-biomaterial fabrication system, a workflow-driven by a customised form-generative and material-distribution computational algorithm was created, whereby robotic extrusion was informed by environmental data. The aim was to provide an agile tool for designers to integrate material performance, digital computation and human intention. Laboratory data on material properties was extrapolated into a computational logic where environmental data was embedded to create a virtual prototype with variable forms and applications. To bridge with fabrication, experimentation was running in parallel with the aforementioned methods in a workshop setting, to ensure manufacturing limitations were constantly considered. Both scientific and design methods with generative and analytical tools were applied in a hybrid research that contributes to the scale of an artefact and a generalisable application level (Groat and Wang, 2013) The complex nature of biomaterials requires a multi-stage approach (Fig. 1).

As an application of the customised design-to-fabrication workflow, the goal was to develop a design for light-filtering wall panels that have bioreceptive and hygroscopic properties. By capitalising on the materials' short lifecycle and biodegradability, the focus is the design of "temporary and highly ecological architectural - scale parts" capable of interacting with the environment (Mogas-Soldevila et al., 2014). Seasonal structures like louvers and sun shaders, for example, can now be designed employing alternative material options. To support future work on animate structures, a material palette was selected on a case study of cyanobacteria, *Oscillatoria animalis*, cultured in hydrogel for photosynthetically mediated biomineralization of calcium carbonate (Tamuli et al., 2021).

2. Materials & methods

2.1. Biomaterial formulation

Three biomaterials were developed using two categories of materials: biopolymers and aggregates. Biopolymers contribute to the creation of hydrogels with various viscoelastic properties while aggregates are added to the

hydrogel formation, to create bulk and improve the compound's overall performance and structural properties (Fig. 2). The biopolymers used were kappa carrageenan, methylcellulose and sodium alginate. The aggregates chosen here are silica sand and wood flour, the triple-filtered, ~0.5 mm wood residues of milling and sanding processes. Silica binding to the best-performing hydrogel composites was tested in crystal form of sizes ranging from ~0.5 mm powder to ~40 mm crystals. Properties of strength transparency-responsiveness upon hydration were observed with alginate and methylcellulose composites whereas kappa carrageenan layers adhered to each other only when the crystals were in powder form. Fine grains resulted in compounds of the highest printability. Different hardwood and softwood mixtures were successfully tested, based on availability at each iteration of material preparation.

2.1.1. Material composition and preparation

To form the multi-biomaterial structure, three material blends were examined in the course of this study (Fig. 3). The final compositions (Fig. 3D and E) were determined through a set of water containment concentrations and aggregates mixing and deposition tests, to achieve homogenous printable compounds. All compositions were prepared in aqueous mixtures. Deposition methods were compared to mixing methods in a series of experiments summarised in Fig. 2.

- Material A — k-carrageenan: SiO_2 crystals [1:1] (Fig. 3A). The final concentration rates of material A ingredients were set to 4% [w/v percentage]. Other rates tested were 3:2 [6% k-carrageenan and 4% SiO_2 crystals] and 2:1 [8% k-carrageenan and 4% SiO_2 crystals]. This was done to enhance the volume of the dried sample by reducing the initial water percentage, but it led to material cracking and elasticity loss. The selected composition is printable and able to maintain surface and texture resolution after dehydration. Glycerol addition is a common practice to enhance elasticity (Zhu et al., 2018) and thus reduce cracking upon dehydration. Glycerol addition was also tested in samples of K-carrageenan mixed with SiO_2 powder. However, to maintain the biocompatibility of the hydrogel element glycerol was omitted from the final formulation.
- Material B — methylcellulose:alginate [12:1] (Fig. 3B). The final concentration of material B components is 6% methylcellulose and 0.5% alginate. Although other formulations of alginate-based materials were more appropriate for extrusion of algae-laden hydrogels in terms of viscoelastic properties (Malik et al., 2020) this composition is optimised for the cultivation of the cyanobacteria *Oscillatoria animalis* in terms of cell viability and growth rates (Tamuli et al., 2021). One drawback is that this composition is not printable without $CaCl_2$ cross-linking since the shape is lost a few minutes after extrusion. While silica crystals and silica powder were tested to improve printability, they reduce layer adhesion and increase brittleness upon dehydration compared to compositions without silica. Therefore, the composition was fixed to methylcellulose and alginate, which increased layer adhesion.
- Material C — wood:methylcellulose:alginate [24:6:1] (Fig. 3C). The final concentration rates of material C ingredients were set to 24% wood flour, 6% methylcellulose and 1% alginate. The proportion of wood flour was critical. When decreased below 24%, the printability was low, although material spread was reduced. The addition of alginate improved print fidelity in low percentage wood mixtures but three-dimensionality was not preserved over time.

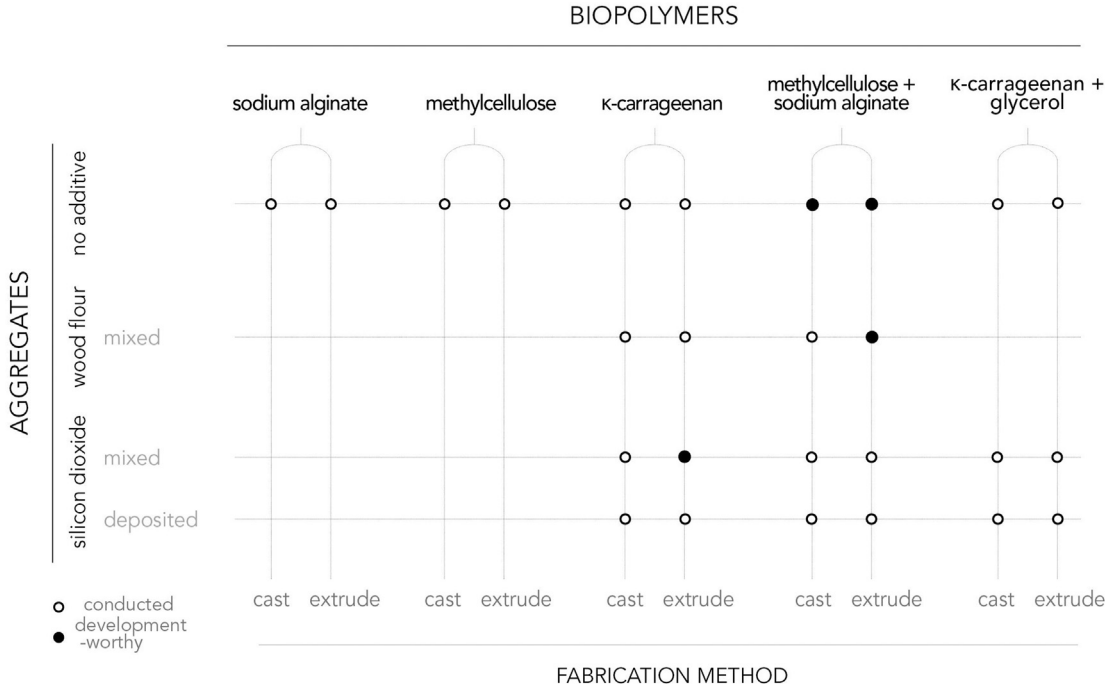

Fig. 2 Experiment sets of biopolymer powders and additives combinations to finalise material composition. Respective explorations of the appropriate fabrication method, casting or extrusion.

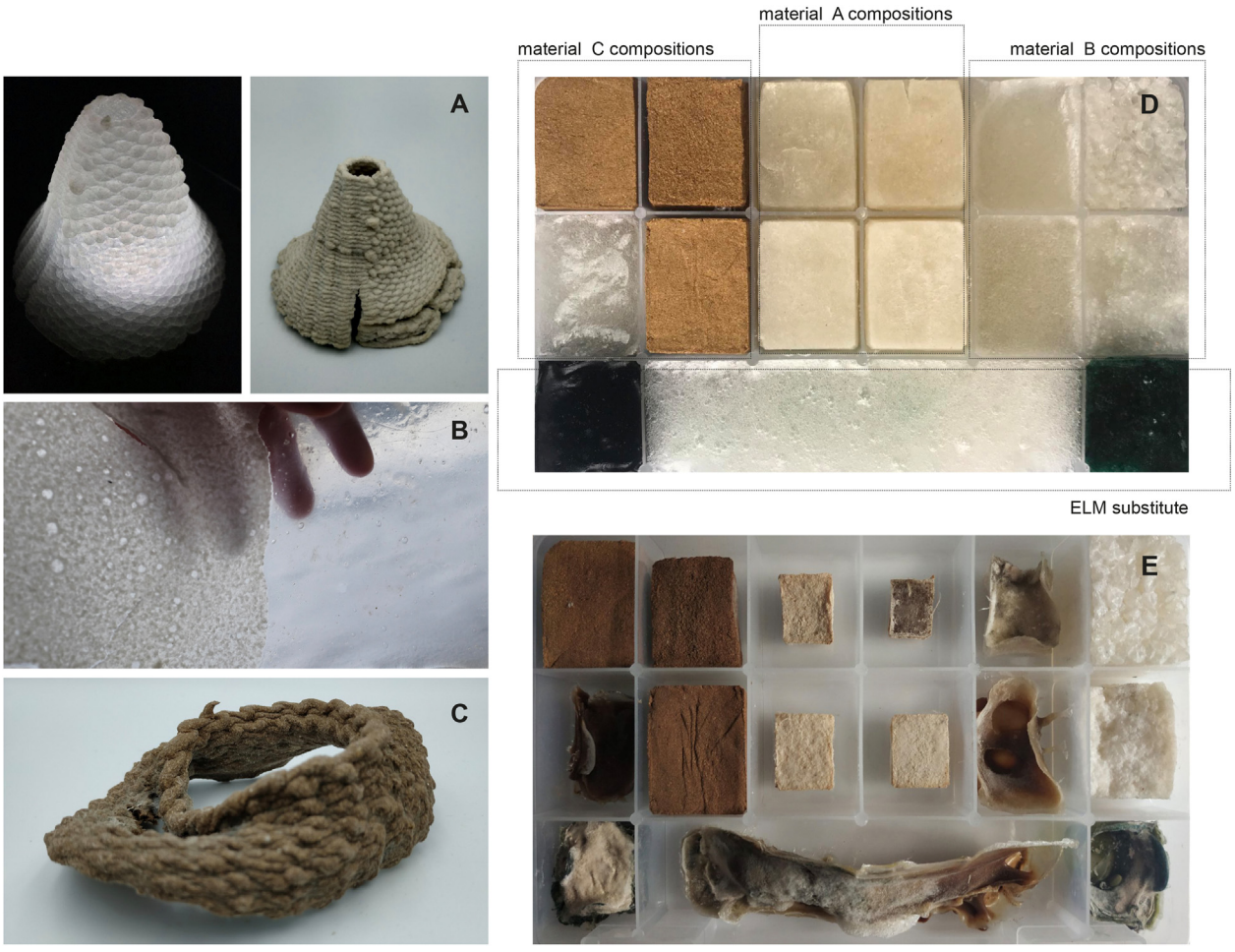

Fig. 3 Final material compositions. Material A, kappa-carrageenan and silicon dioxide material B, left: methylcellulose and alginate with integrated silicon dioxide powder right [A]: final methylcellulose and alginate composite. [B] material C, methylcellulose, alginate and wood flour [C] finalised material palette [D-E] wet [D] dried [E] and respective optical gradience of the proposed materials.

2.1.2. Composite properties

Water-based biomaterial printability is characterized by a series of rheological properties which include shear thinning, viscosity, yield stress (Liu et al., 2019), and swelling behaviour (Kim et al., 2019). For non-Newtonian fluids such as the developed biomaterials presented here, shear-thinning properties allow materials to flow easily via the printer nozzle (Liu et al., 2019). Mass flow rate calculations were conducted under steady pressure conditions summarised in Table 1. Evaluation of manual prints (Fig. 4A) was conducted to assess viscoelastic properties and printability. Water absorption was the parameter that caused transparency gradation for materials A and B. Material A was also displaying hygroscopic swelling and water-containment capacity upon absorption. A dome structure prototype of 100 mm original diameter was partially submerged in water and then left to dry naturally, and material transparency and shape changes were documented (Fig. 5). Material C had negligible changes upon water absorption and was therefore considered as a structural material. The profiling parameters are summarised in Table 1. This ability to create responsive optical gradients was important both to the function of the proposed, light-filtering wall element, as well as biocompatibility with photosynthetic bacteria.

To understand the impacts of ambient conditions on material properties (Fig. 5), a humidity and temperature data collection sensor DHT22 AM2302 was utilised with an accuracy of $+/-2\%$ for humidity and $+/-0.5$ °C for temperature. It further included an Arduino Uno board. Readings were successfully imported into *Grasshopper* via the *Firefly* plug-in (Payne and Johnson, 2015) which enabled real-time data imports, updates and data recording.

2.2. Computational algorithm and data integration

To deal with the challenges of computational designing and digital fabrication of heterogeneous structures (Duro-Royo et al., 2015), a seamless workflow with integrated material, design and fabrication processes was created. This was achieved by transferring material properties from physical to digital through colour coding and clustering. The geometry was approximated by a set of minimum printable units and each biomaterial represented by a different colour,

Table 1 Characterisation parameters for fabrication of the material library.

Material	Purpose	Dynamic properties	Water solubility	Mass flow rate (g/s)	Steady pressure (bars)	Speed (mm/s)
A	Water containment	Transparency, shape	Low	2.21	0.35	8
B	Binding, cell growth	None	High	1.57	0.75	1
C	Structural enhancement	None	Low	2.67	5.1	2

enabling the generation of a series of spatial arrangements which were environmentally informed. Therefore, a three-stage computational algorithm was developed. The first stage included an interactive evolutionary algorithm with inserted geometrical and variance rates. At this point, other fabrication parameters were introduced as constants: the layer height and the minimum distance between targets, which were defined by the selected nozzle size and tool motion speed. At the second stage, environmental analysis data was inserted. Exposure to solar radiation dictated regions of optimal conditions for cell growth, hence ensuring the structure's biocompatibility. Solar exposure is an incremental type of data in the context of light-filtering, potentially photosynthetic cell-bearing structures (Fondriest Environmental, 2014). Concurrently, this analysis highlighted areas of low exposure to sunlight — less than 4 h-which required increased material A volume concentrations to promote future growth. This material acted as a hydrating agent due to its water-absorbing capacity and potential to increase water potential for microorganisms upon hydration. In these regions, material B concentrations should also be reduced or even avoided, to avert the embedded living cells' non-viability. Solar heat gain was an equally important factor to be measured. Rising temperatures of a surface structure have a direct effect on the water containment, as well as the viability of the cells. Specifically for *Oscillatoria animalis* cultivation, inoculation should be avoided in areas that display temperatures greater than 25 °C. Solar data was chosen amongst other types of environmental data to be integrated into this study, due to the proven light intensity effect on the pigmentation of the cyanobacterial biofilm (Tamuli et al., 2021). The third step of the algorithm was the merging point of all analytical and fabrication data. This step introduced a Machine Learning Algorithm (MLA) that clustered data based on the environmental analysis attributes. This algorithm is embedded in a Grasshopper node available through the LunchBox plug-in (Miller, 2020). For this workflow, a Gaussian Mixture Model was preferred over a K-means Model and a Naïve Bayes classification model. This choice was driven by the former model's ability to group data into homogenous components that represent data set tendencies more accurately (Miller, 2019). Although the computational costs are higher in the case of the Gaussian Mixture Model, the result was of higher resolution. The unsupervised MLA was provided with two datasets. It detected patterns to generate two clusters of discrete colour encodement, representing materials A and C. This data was consequently transferred into the G-code generating part of the algorithm to produce a machine-readable file. This G-Code generation was based on a C# script (Hughes, 2019) modified by the authors according to the available CNC machine.

Subsequently, a detailed, step-by-step overview of the developed computational algorithm was presented, which bridged the parametric design capacity of *Grasshopper* software with the limitations of fabrication. In step 01 (Fig. 6), the interactive evolutionary algorithm produced a set of design options. The variable parameters/genes reflected the orientation and scale of the defining geometry curves. Then a set of new parameters were defined to act as selective tools of evolution, including the design's

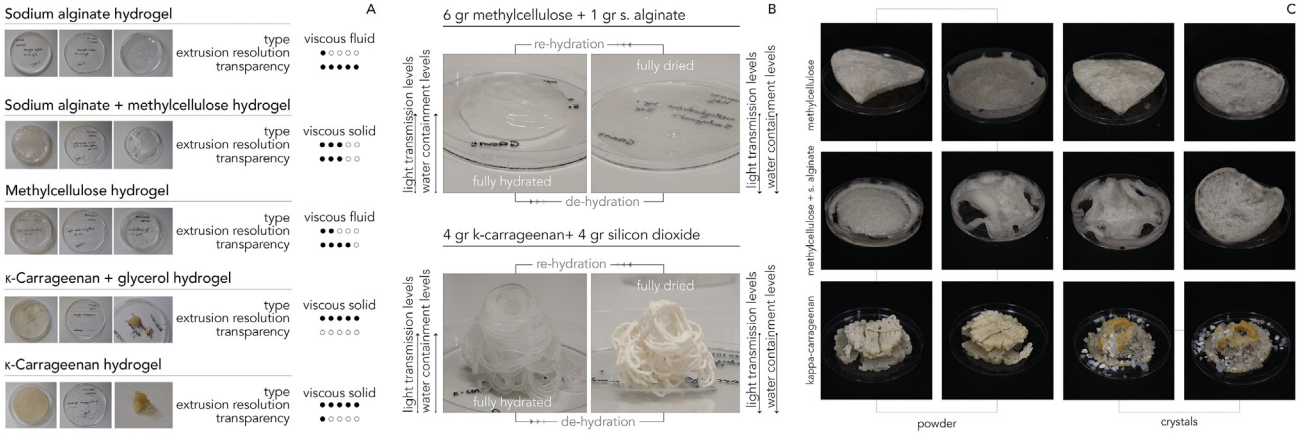

Fig. 4 Qualitative evaluation of best-performing compositions: viscosity, printability and transparency [A] properties of material A and B upon hydration and dehydration [B] Silicon dioxide inside pre-mixed hydrogels in crystals and powder form [C].

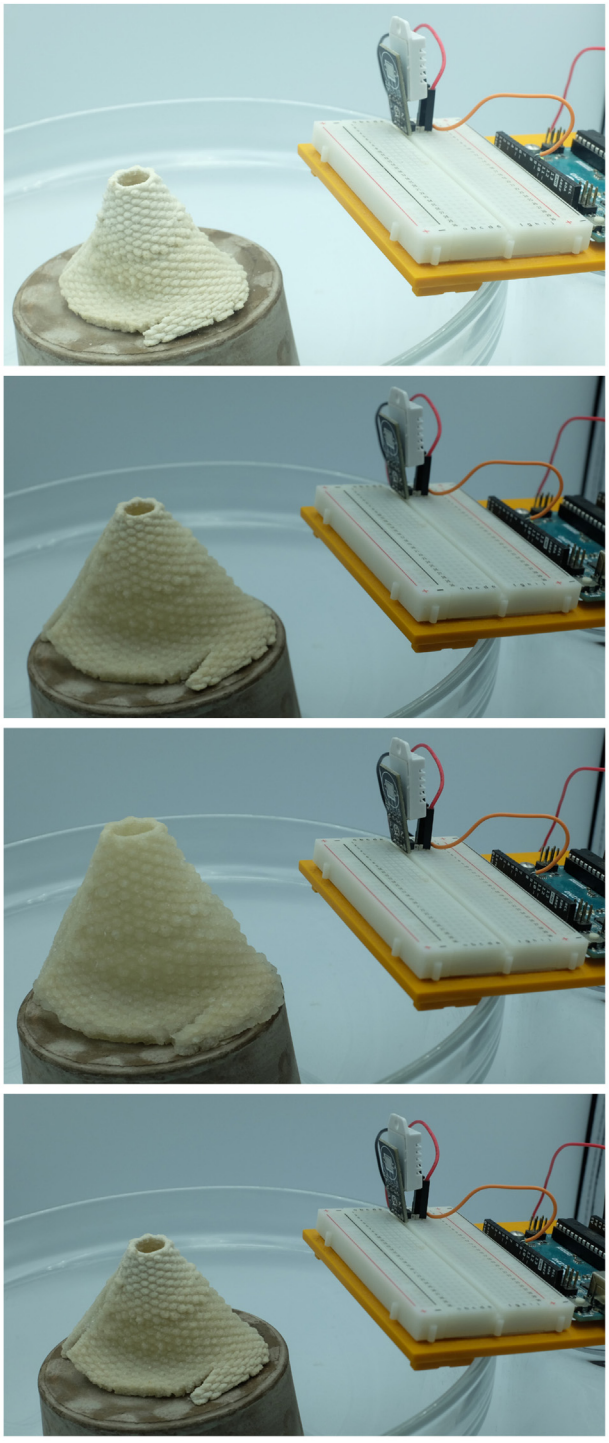

Fig. 5 Material A responsiveness. Rehydration of dried sample and micro conditions recording with Arduino board and DHT-22 sensor.

toolpath resolution, meaning the total number of target points, which should remain low to produce a light G-code file. This in turn was readable by the CNC extruder and the variance of each gene, to capture the vastest area of possible formal outputs. The evolutionary algorithm was available via the *Biomorpher* plug-in (Harding and Olsen, 2018) and differed from traditional evolutionary optimization algorithms like *Galapagos* (Rutten and McNeel et al., 2009) as it allowed to select which design outputs were supposed to promote from one iteration/generation to the next. In that way, the result was a combination of top-down, deliberate design intensions and bottom-up self-generative computational evolution of the software. The fabrication-driven optimization in step 02 was based on physical tests, which proved that curvilinear geometries performed better upon natural curing (Fig. 6). Therefore, the orthogonal input geometry underwent a physical-based deformation simulation with the help of *Kangaroo* plug-in (Piker, 2017) for *Grasshopper* (Rutten and McNeel et al., 2009). To create an environmental analysis friendly mesh inside *Grasshopper* in step 03, the geometry underwent a maxel - material and voxel - approximation process as described previously (Oxman, 2013). The advantage of using maxels allow to define the size of voxels according to the respective fabrication set-up parameters. The voxel size could be adjusted to the required level of analysis and/or printing resolution which had the minimum maxel size and highest resolution of 3 mm $\times$ 3 mm $\times$ 3 mm, given that the nozzle diameter was 3 mm.

This maxel approximation process allowed for computationally efficient solar radiation and solar heat gain analyses to be conducted in step 04 (Fig. 6). The total number of sun exposure hours per unit area, namely per mesh face was calculated by a customised *Ladybug* component in *Grasshopper* (W-LAB, 2021), whereas the external solar heating effect was calculated in *Autodesk CFD* (CFD Product team, 2019). The resulting temperature values were imported into *Grasshopper* encoded as a CSV UTF-8 file. Both analysis data were imported into a clustering MLA to define the distribution of the materials. Two clusters were created, which represented materials A and C. The last step of the computational algorithm regarded the generation of the materially informed toolpath. The tool target coordinates and the solenoid valve portal position were defined following the previous step of the material assignment.

2.3. Pneumatic extrusion setup

A pneumatic extrusion process was followed for fabrication (Fig. 7A and B). A single pneumatic extruder was attached to a CNC milling machine for the prototypes. The envisioned fabrication system with a multi-nozzle end effector attached to a UR10 robotic arm is presented in Fig. 7A. A 3 mm nozzle was used, to ensure adequate printing resolution and a line thickness that allows for detailing to the desired level of quality using parameters defined in Table 1. For the fabrication of the final prototype, the optimal distance of 2.5 mm from the printing base for the first layer coincided with the defined layer height of each consecutive layer.

2.3.1. Material compatibility for large scale multi-biomaterial extrusions

To scale up from the initial object scale, prototypes of dome-shaped structures with material distribution methods were tested. The following parameters were defined as critical for a successful result: the direction of material deposition in relation to the upper and lower layers; the

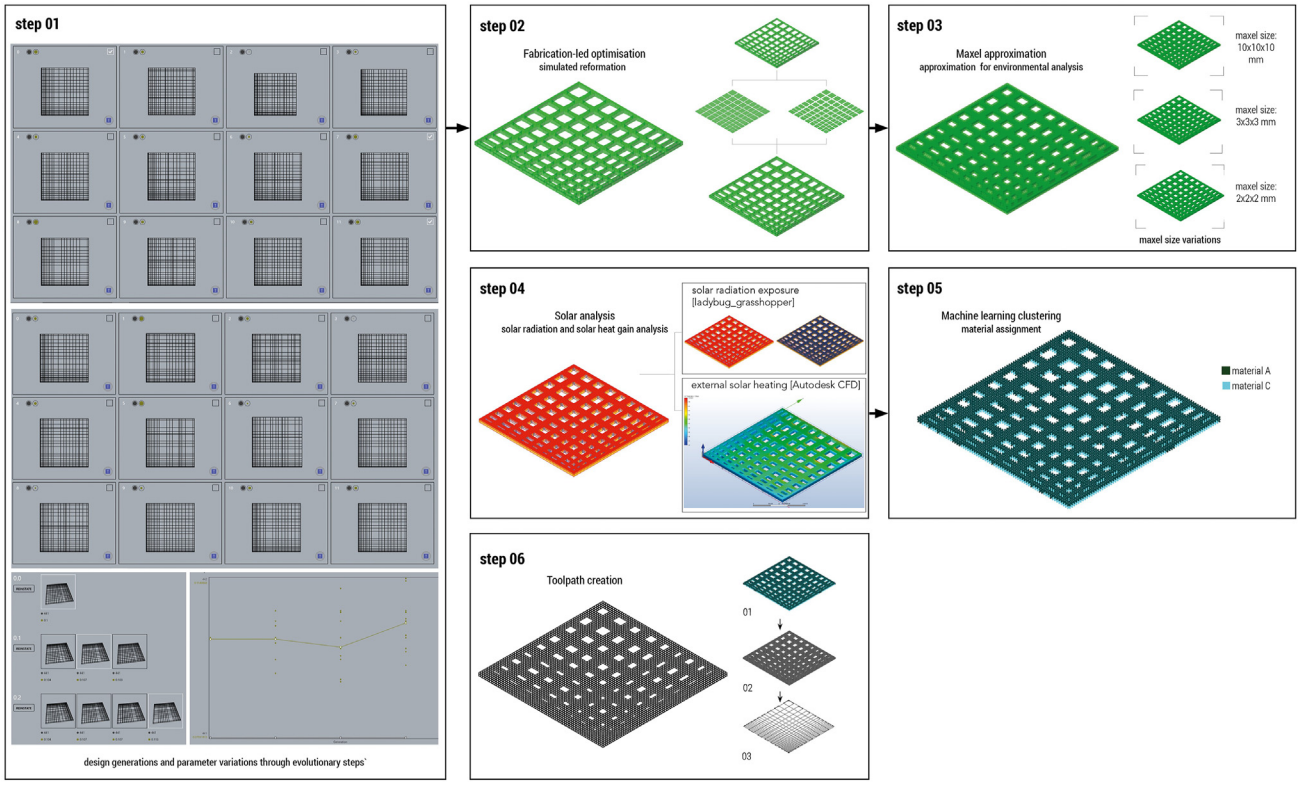

Fig. 6 Step-by-step computational workflow overview.

Fig. 7 Robotic multi-biomaterial pneumatic extrusion set-up [A] end effector close-up [B] multi-biomaterial deposition direction: vertical [C] diagonal [D] horizontal [E].

adhesion to other materials; and the gradient of volume concentration. The materials deposition was tested successfully under three different directions: vertical, horizontal and diagonal (Fig. 7C—E). Here, material deposition direction refers to the spatial relation between the extruded material layer and the layer directly below it (Fig. 8). To define successful adhesion between materials, preliminary test extrusions were conducted, regarding all possible two-material combinations. Materials A and C displayed poor adhesion upon drying. On the contrary, Material B adhered fully to materials A and C upon dehydration. Therefore, regardless of the material deposition direction, material B was necessary between A and C. Given its binding properties and slower curing time, there was less shrinkage between different materials. Subsequently, a set of large-scale iterations were designed. They created defined parameter settings for large-scale prototypes of 840 mm × 470 mm (Fig. 9C), as the material deposition direction and geometrical complexity were posing challenges during upscale. Due to the increased complexity and number of parameters, the integration of environmental data at this stage was omitted. Observations from small scale tests were integrated into the geometry of the final designed pieces. For the printed test presented in Fig. 9, only material C was utilised. This material was the most structural and less deformed upon dehydration of the

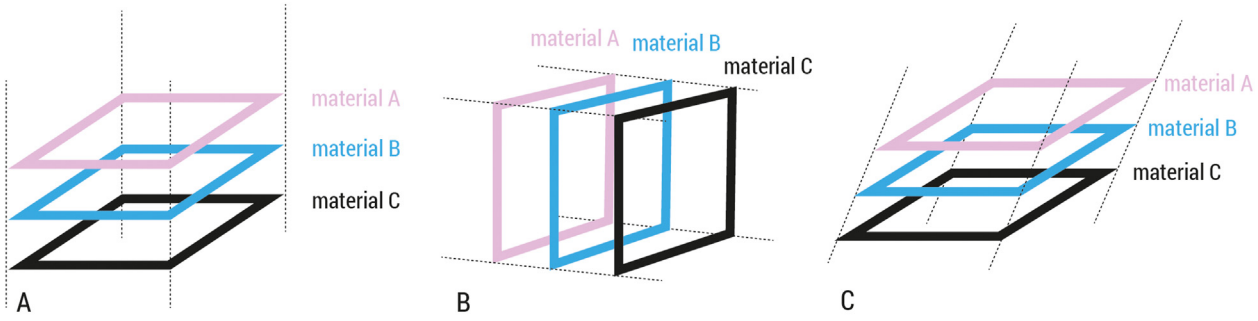

Fig. 8 Material deposition direction: horizontal [A] vertical [B] diagonal [C].

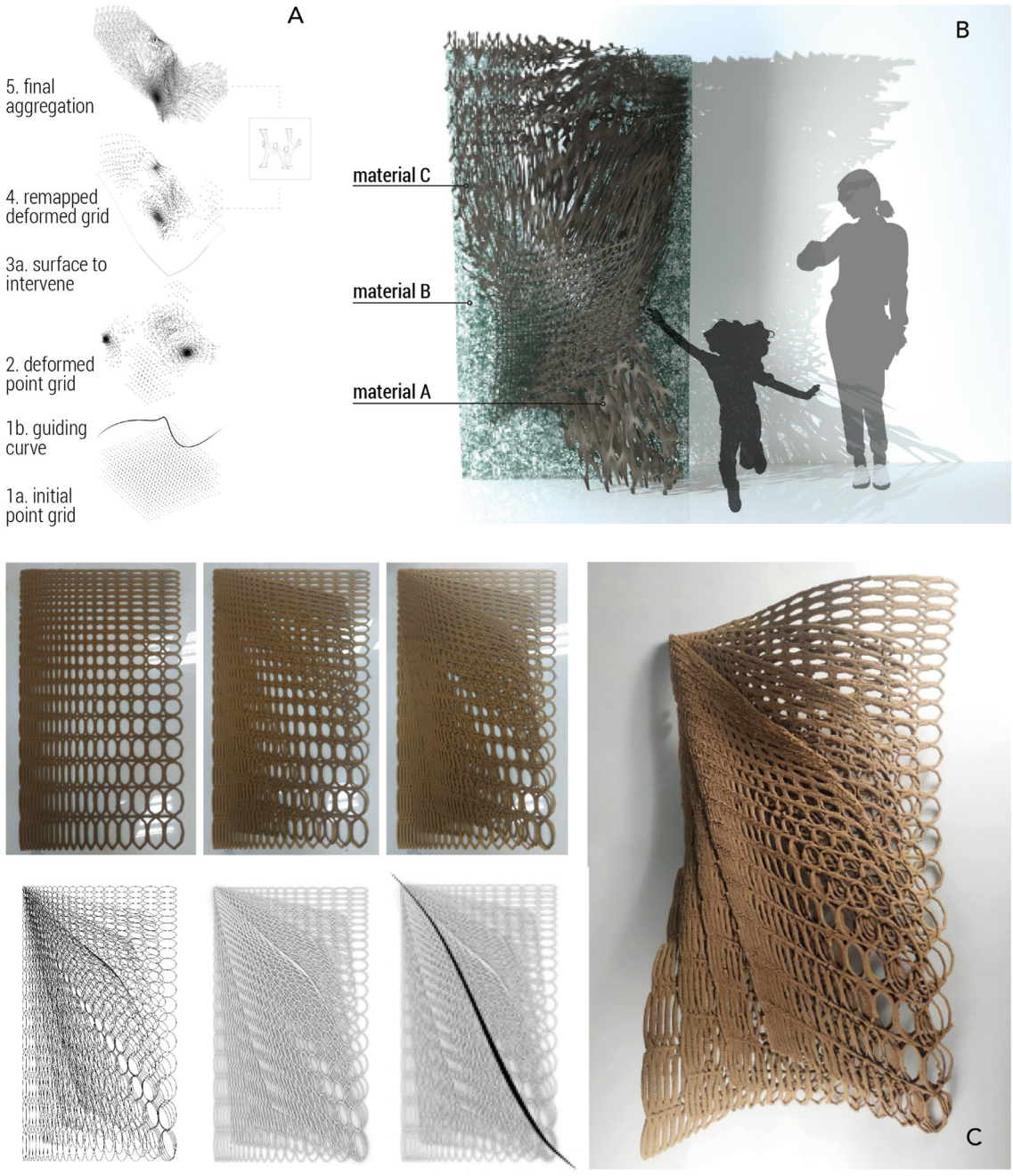

Fig. 9 Large-scale prototype articulation of computationally analysed element [A] visualisation of the proposed wall panel [B] simplified version of panel geometry and layer-by-layer deposition of material C [C].

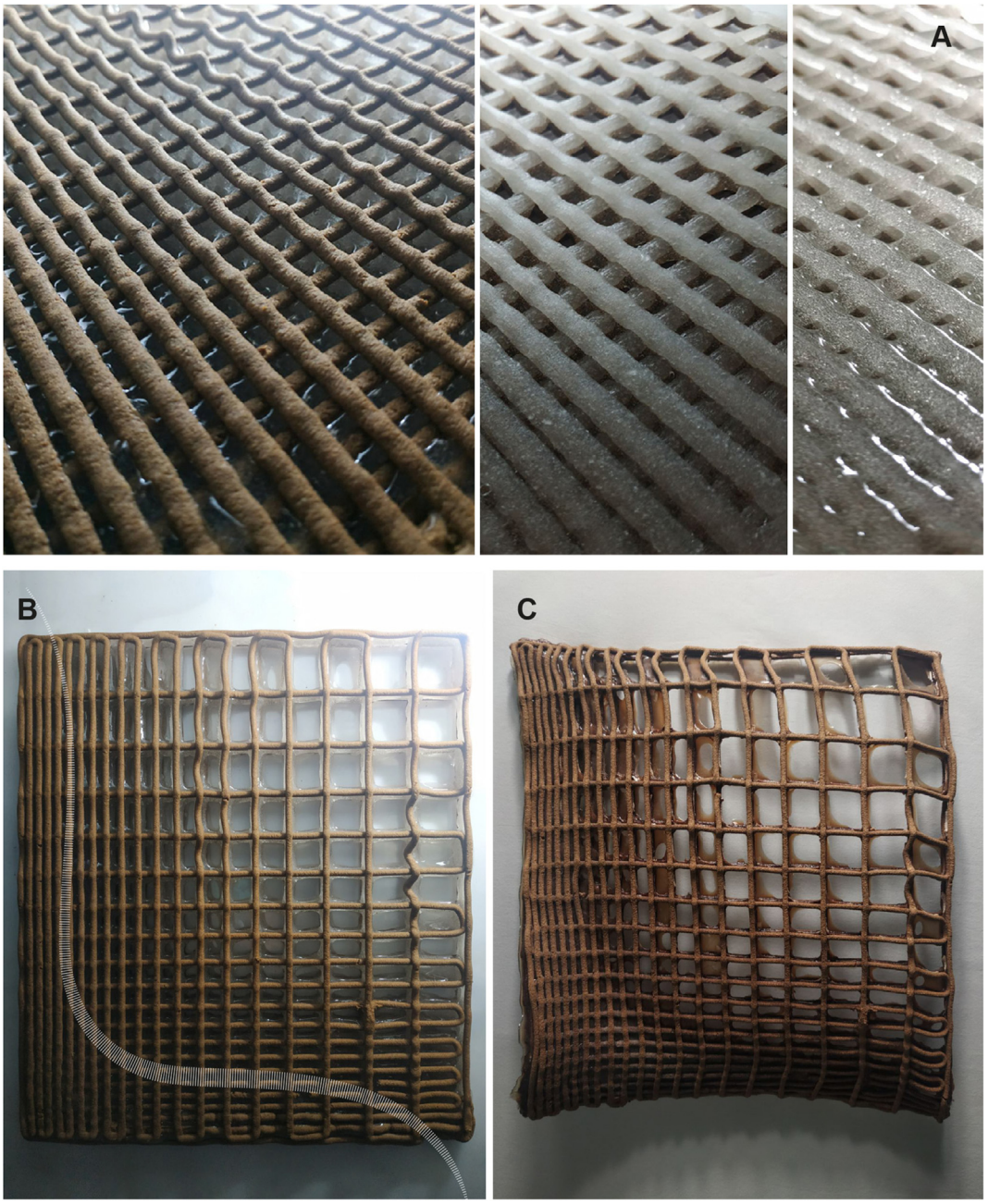

Fig. 10 Horizontal multimaterial deposition direction. Layer 01 - material C, layer 02 - material B, layer 03 - material A, layer 04 - material B, layer 05 - material C [A] extruded prototype [B] dried prototype [C].

three, and was solely used in this prototype. This created a proof of concept for the original hypothesis that the varying material volume density along a surface would result in a guided deformation of the flat extruded geometry upon drying. The double curvature of the prototype resulted from the natural drying process of the volumetric gradient, occurring on a 4-layer, flat upon extrusion surface (Fig. 9). A complex pattern was designed using an aggregation parametric model (Fig. 9A) that followed the process presented previously (see Supplementary material). Subsequently, the pattern was simplified to an irregular grid of distorted ellipses. The black curve on Fig. 9C represents the predicted spine of the surface — the area with the highest volume density, thus the most limited deformation. Deviation from the curvature denoted greater deformation. The same hypothesis was proven for all three materials through a geometrically simplified irregular grid prototype (Fig. 10), which combined all materials according to their regional volume concentration. The third, more complex output (Fig. 11) regarded a 6-layer, printed flat surface, which combined the deposition of all three materials in a diagonal direction. The volume density was again variable, and the centroid of each layer was packed between two layers of material C. It created a controlled deformation towards the panel centre and a gradually greater one towards the panel edges.

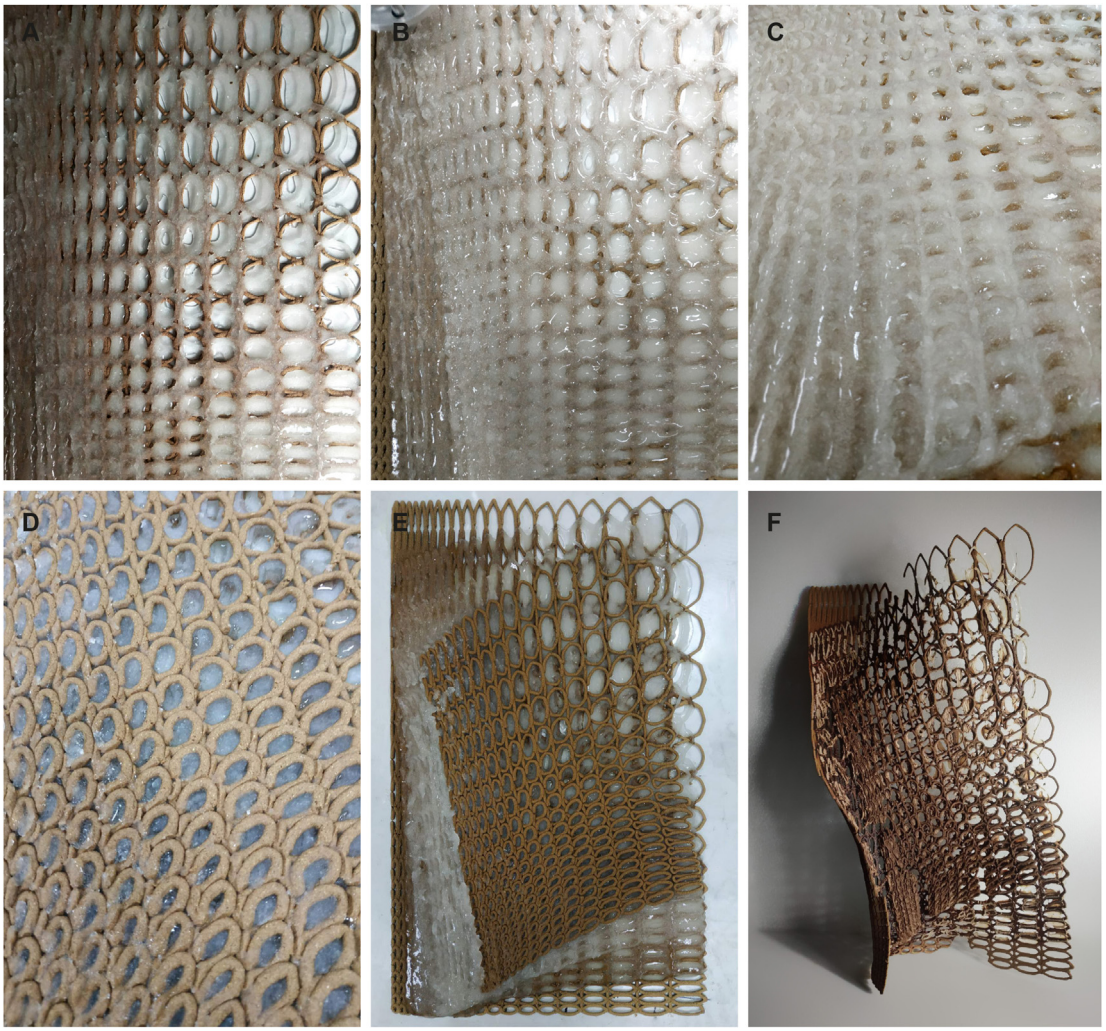

Fig. 11 Diagonal deposition direction. Layer 01 - material C, layer 02 - material B, layer 03—04 - material A, layer 05 - material B, layer 06 - material C [A-D] printed prototype [E] dried prototype [F].

2.3.2. Contextualisation of material performance and fabrication application

In the case of open-air printing, environmental conditions such as temperature and humidity may challenge the structural stability. Exposure of responsive biomaterials to real conditions that may differ from the values of controlled room conditions could lead to structure failure both during printing as well as upon drying. After conducting preliminary printing tests, including those presented in Section 2.3.1, the following observations were made: Temperature values above 35 °C led to a change in material viscosity and a radical reduction of natural curing times, resulting in printing inconsistencies and uncontrollable shrinkage upon drying. Materials A and C performed as predicted for all conditions ranging between 16 °C and 35 °C. These observations rendered the definition of optimal conditions for each material extrusion necessary using a bespoke setup (Fig. 12). In addition, the heat index values were collected, as a difference greater than 5 °C between temperature and heat index could lead to alterations in the hydrogel's viscosity and an unpredictable material behaviour. In summary, the extrusion process should be avoided above the limit of 35 °C for material constraints, and 25 °C for biological stress.

3. Results

Following the described workflow, a porous wall panel prototype of 350 mm × 350 mm was fabricated (Figs. 14 and 15) using materials A, B and C. Data derived from solar radiation and heat gain was measured in the Southern Spanish city of Cuenca. The site was chosen as a representative of the Mediterranean climate as it suggests multiple applications for shading devices. Weather information was drawn from publicly available datasets.

Water absorbance reduced the mechanical strength of all materials thus leading to structural collapse. While all materials returned to their initial gel state, material B proved to be structurally the weakest one. Material A exhibited shape-memory capacity up to six cycles in the conducted response reversibility tests. The dome prototype was doubled in height and diameter between the dry and wet state, while a noticeable transition from translucent to

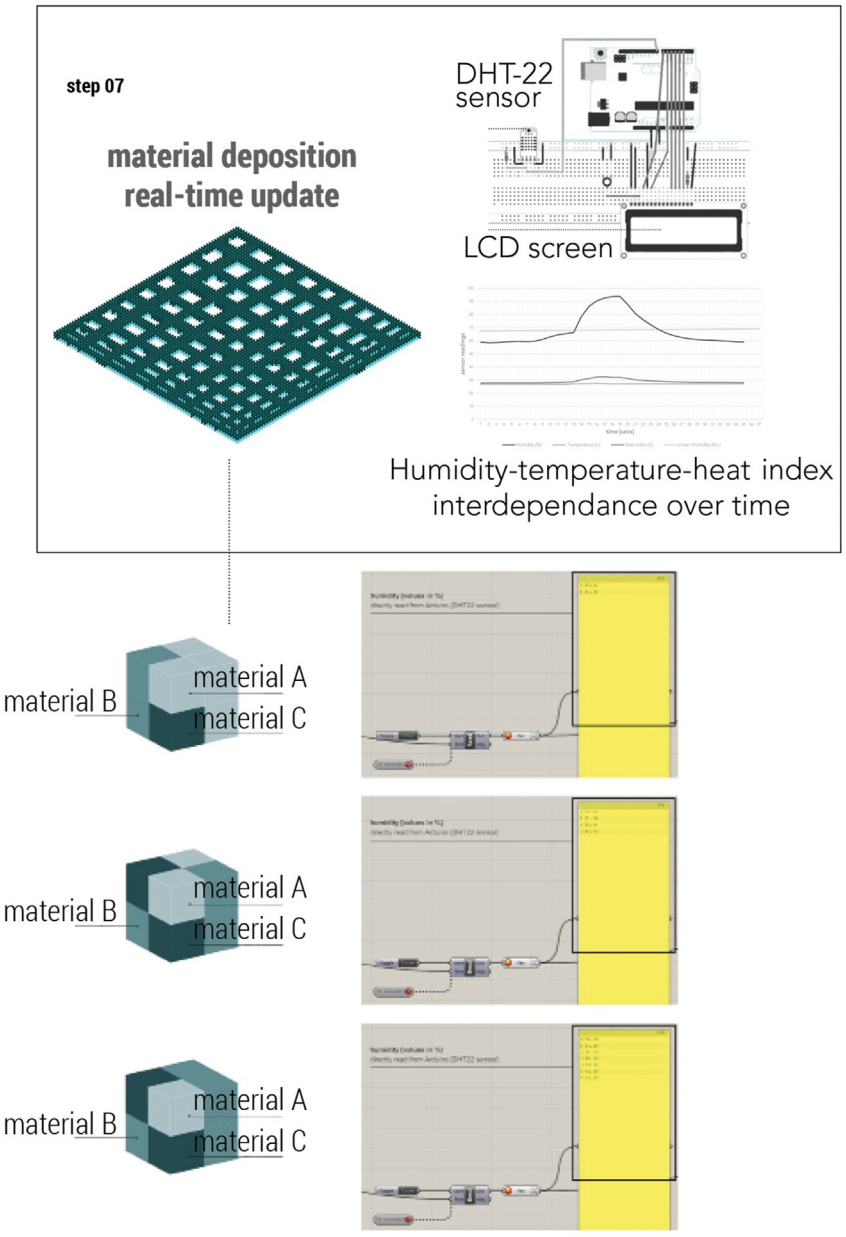

Fig. 12 Arduino DHT-22 sensor set up, Grasshopper live sensor readings import and recording of temperature data.

transparent properties was also documented (Fig. 5). Following that, the integrity of the structure was reduced and the resolution of printed textures demoted in every cycle. The water absorbance capacity was further reduced in following cycles, from 6.6 times the material's weight during the first cycle to approximately 5.2 during the second cycle. At the same time, silica crystals displayed reversibility of response greater than twenty cycles. By integrating Material A into the structure, the vertical transfer of water was achieved without the need for mechanical systems. By controlling its place in the structure, moisture levels across the scaffold were controlled and differentiated both in a vertical as well as a horizontal axis. Only small amounts of sprayed water (approximately 250 mL) were successfully absorbed. On the other hand, the prototype in a dried state exhibited self-supporting capabilities which proved to be important to be successfully attach to an existing wall. Despite these limitations, the proposed biomaterials lifecycle (Fig. 13) renders them an agile candidate for future biomaterial applications.

To refine the computational workflow further, in some tests the fabrication-led optimization processes was excluded based on the deposition directionality and materials utilised. This proved that the computational workflow had the agility to omit steps and to include both other types of analysis data without failing to produce an output. At the same time, two different resolutions for the same grid lattice (Figs. 14E—15E) were compared, a high one of 10,292 maxels (Fig. 14A), and a low one of 377 maxels (Fig. 15A). This difference of resolution was depicted in the computational cost of each analysis. As a proof of concept, the analysis was restrained to one summer day, 01/06, both

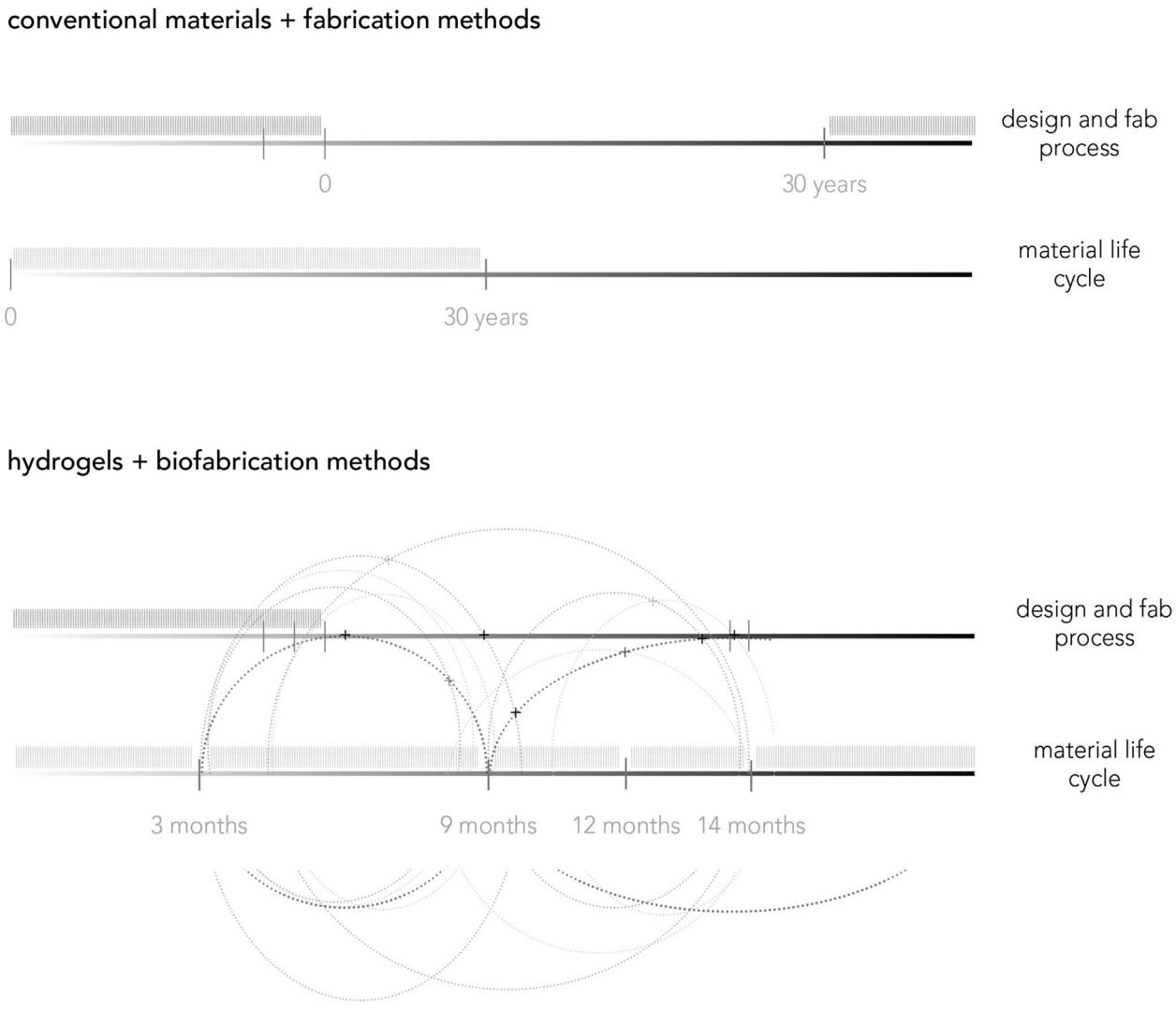

Fig. 13 Lifecycle comparison between conventional materials and hydrogels and respective fabrication methods.

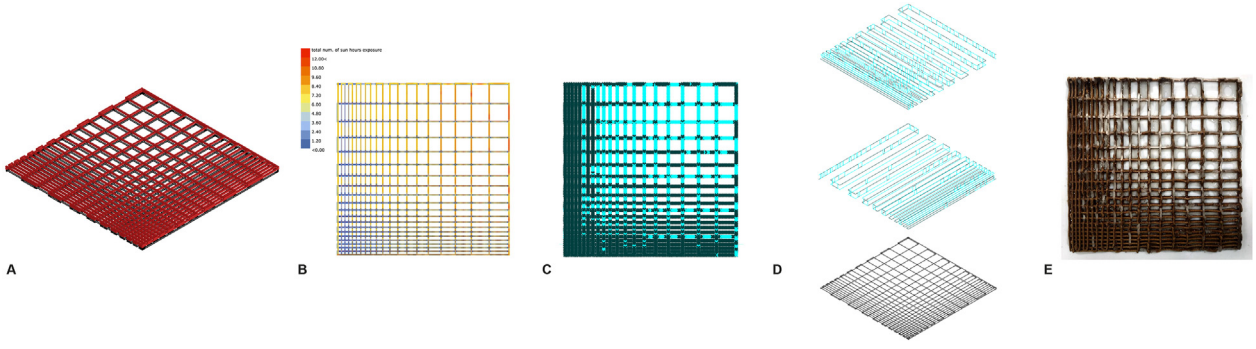

Fig. 14 High-resolution maxelisation of grid geometry - 10,292 maxels. Maxelisation [A] total number of sun hours exposure analysis [B] Machine learning clustering result [C] toolpath creation [D] pneumatic extrusion result [E].

in *Ladybug* and *Autodesk CFD*. On an intel i-7, the high-resolution model demanded 40 mins for the *Ladybug* and approximately 120 mins for the *Autodesk CFD* tool to run. On the same setup, the low-resolution model demanded 10 min for *Ladybug* and 40 mins for *Autodesk CFD*. When merging environmental data as attributes in the MLA, the data list's length had to be equal. Additionally, the length had to be equal to the maxel's total number. To achieve this, a mass addition of the analysis resulting points and values was run. Data was merged in groups of six - as each

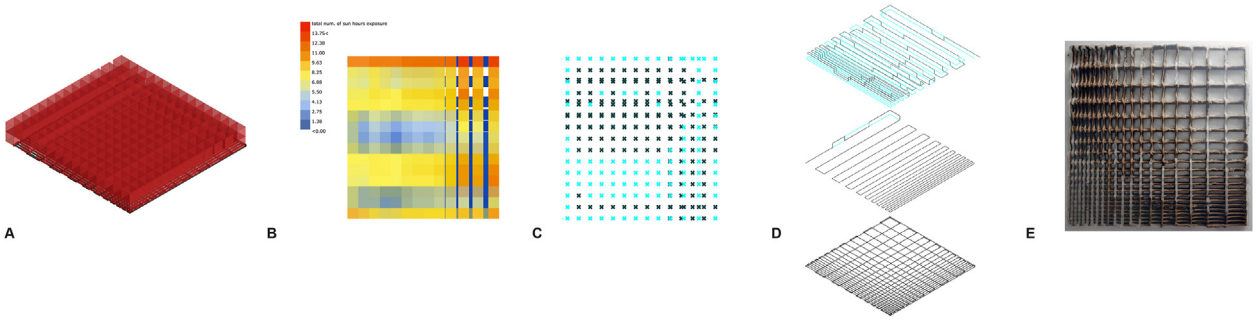

Fig. 15 Low-resolution maxelisation of grid geometry - 377 maxels. Maxelisation [A] total number of sun hours exposure analysis [B] Machine learning clustering result [C] toolpath creation [D] pneumatic extrusion result [E].

maxel has six faces, and therefore six values of total sunlight exposure hours. A similar logic was applied to *Autodesk CFD* post-analysis exported nodes. The list length of node values was divided by the maxels number to define the length of each group value that was averaged. This was necessary due to the different meshing processes followed inside the two softwares. Alternatively, it could have been resolved via coded, custom-based meshing. For the MLA, the data sets used as attributes were: 1) the total number of sunlight exposure for each mesh face, and 2) solar heat gain. In Figs. 14C and 15C the result of the algorithm is the two-coloured point clusters representing the two materials - light blue stands for material A and dark blue for material C.

In order to translate the colour coded points of Figs. 14C and 15C into a fabrication toolpath, a procedural adjustment was required to achieve the multi-material printing with a single nozzle. Each material had to be deposited individually per layer, leaving space for the second material to be deposited afterwards (Figs. 14D and 15D). Subsequently, a set of extra points were created to act as initialisers and stoppers for the air supply. Due to the material's differences in viscosity these extra points were at a different distance from the start/endpoints of the printed geometry. All materials were extruded with the speed and pressure values defined in Table 1. For material A the air pressure supply was activated 5 mm higher than the starting target point and deactivated at the ending target point. For material C the air pressure supply was activated 8 mm higher than the starting target point and deactivated 0.5 mm higher than the ending target point. Material B was extruded following a continuous toolpath; consequently, no extra points were defined. The results of the tests (Figs. 14A—15A) showed that the same solar data can create two different distribution results (Figs. 14E—15E), proving therefore that customisation is not only an environmentally but also design-driven process.

To ensure structural integrity, however, high concentrations of more viscous materials A and B in continuous vertical layers were avoided, as it led to structural collapse. A deposition pattern of repeated changes of materials was implemented instead. Regarding the deposition directionality, the vertical direction offered a greater resolution and structural performance. Nevertheless, the diagonal deposition direction allowed for a greater surface area of each material to be exposed to open-air, rendering its responsive performance greater at scale and intensity. In general, the large-scale experiments confirmed that enclosure of materials A and B between layers of material C (Fig. 9A and B) leads to more structurally successful and mechanically robust results compared to the rest of the methods tested.

Natural drying is affected by the extruded line thickness, material volume and its overall spatial distribution. These relationships also affect the occurrence of cracks upon dehydration due to uneven drying across different regions of the structure. The complex co-existence of multiple material, environmental and fabrication parameters for predictable deformation was accepted throughout all experiments with the following techniques used to address it. A silicone lubricant film was applied to help resolve the challenge of printing base friction. Curvilinear geometries displayed fewer failures relative to polygonal as they minimise changes in the CNC motion axis. During printing the delay at corners caused the extruded paths to have an irregular thickness which was the result of directional changes and tension forces that derive from differences in drying times. Material C displayed negligible failures in both curvilinear and linear cases, but Material A performed better in curved formations. Greater volume per area led to less deformation due to the reduction of the contained water volume. Consequently, the volume gradience led to a gradient deviation from all three x, y, z axes. This behaviour was confirmed for both single and multi-biomaterial experiments. Especially, in cases where Materials A and B were not contained between layers of Material C, shrinkage tensions became unpredictable, leading to extreme deformation and finally also to cracking.

4. Discussion

One of the greatest challenges when fabricating with hydrogels and responsive water-based materials is to produce large-scale and replicable lattices in which the shrinkage is controlled and predictable. As observed in this study, hydrogel deformation during natural curing displayed irregularities when performed in an open-air context, as it is a process that relies on moisture evaporation that is dependent on environmental fluctuations of humidity and temperature. The workflow attempted to bridge this contradiction between the high resolution and fidelity of the digital tools and the semi-controllable behaviour of the non-standardised, customised biomaterials. This bridging

has now created a viable design and manufacturing protocol for such new materials to be integrated into architectural design processes and applications.

This research was differentiated in terms of the hydrogel's chemical cross-linking as presented previously (Malik et al., 2020). Chemical insertion was here replaced by an integrated workflow in which design and fabrication strategies act synergistically with material properties. The resulting multi-biomaterial lattices were developed following a process based on results from Duro-Royo et al. (2015). However, the fabrication data and material properties were here integrated into a node-based coding workflow embedded within the software environment of *Grasshopper*. In this way, the proposed method is now available to by a wider audience of designers who do not have scripting knowledge.

The creation of scalable printing with multiple biomaterials offers the potential to examine human interaction with these novel materials. The proposed methodology shifts away from a long-lasting allographic approach in architecture towards new autographic protocols that integrate responsive water-based composites and material

Fig. 16 Articulation of prototypes.

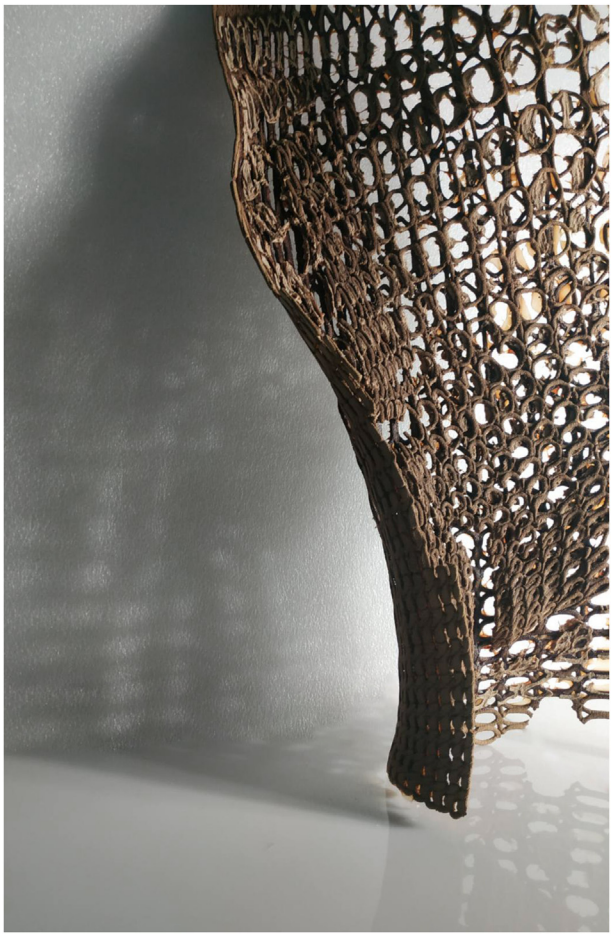

Fig. 17 Multi-biomaterial wall panel prototype of Fig. 9 close-up, showing the dried prototype 20 days after extrusion.

fusion (Grigoriadis, 2018), the latter being possible via the employment of advanced manufacturing and viscous material substrates. The proposal attempts to fulfil "the eight-point syntax of architectural multimateriality" (ibid, 2018) by composing and merging materials instead of discretely arranging them while eliminating boundaries without fully accepting the established "errors of accuracy". Three-dimensionality becomes in this case an emergent characteristic of the lattice throughout its formation process, rather than an allographic interpretation based on predefined drawings. In addition, the proposed algorithm structure generates outputs that blend self-generative computation evolution with the architect's deliberate design choices. By extending the concept of gradience (Wiscombe, 2012) the proposed lattices are understood as a set of 'local regions' within a 'global' structure. Multi-materiality here meets multi-scalarity of performance and response within the time continuum. The novel material palette becomes animate and alive because of its capacity to adapt and respond. The final built prototype acquires a cognitive life (Malafouris, 2018).

On the other hand, working with biomaterials offers the potential to embed microorganisms and create an augmented functionality that is biologically determined. The integrated workflow presented here sets the basis for future animate materials where the variability of conditions will impact biological performance. While *Oscillatoria animalis*, a filamentous cyanobacteria species provided a proof of concept for the presented workflow, other microorganisms could be used in future (Malik et al., 2020) for alternative performative qualities. The workflow agility allows for the implementation of other biomaterials and species, and the customisation to specific functions. At the same time, in future, many more parameters will become embedded into the environmental model, which allows increased levels of accuracy and biological adjustment. Given this, the set-up of the computational workflow allows for the import of other types of biochemical or material property data too. This data could be merged and assigned as attributes into the MLA step, enhancing the computational workflow's agility. Furthermore, light exposure is critical, as well as other types of analytical data derived from cellular growth rates. Surface water run-offs combined with solar radiation exposure could indicate optimal areas for material A to support cell growth in material B. On a hardware level, the directional control valve ports, controlled by the G-code definition, can be live updated to shift air supply to the most appropriate cartridge. For instance, if a temperature value deviation is detected from the DHT-22 sensor, the software prediction will be updated in real-time, thus remaining in line with the actual environmental conditions. When the unpredicted values remain constant outside thresholds, printing will be paused to evaluate the outcome and avoid single material prints. By embedding environmental data into biomaterial printing, not only remote geo- and environmental contextualisation of the structure will be possible, but also manufacturing responses to the living system's needs.

The final large-scale prototypes were designed and fabricated to be used as responsive screens to filter light (Figs. 16 and 17), suggesting environmentally sensitive conditions in buildings. Upon water absorption, materials A and B can potentially change their transparency levels, thus reducing the amount of filtered light (Fig. 5). Indoor spaces are able to vary the intensities of luminosity according to hygroscopic fluctuations of the materials. This variance is dependent on ever-changing environmental outdoor conditions in terms of its relative humidity, in this manner allowing for more permeable, dynamic and responsive boundaries conditions of walls and facades in our built environment.

5. Conclusion

The proposed workflow provides an integrated scale-up approach for the design and digital fabrication of a light-filtering panel system that is composed of multi-graded materials that are spatio-temporally differentiated. Through an integrated design and fabrication workflow, environmentally informed multi-biomaterial structures are able to be driven by the calibration of biomaterial properties and manufacturing techniques. The traditionally static and predetermined material articulation in design is proposed as a more agile process, informed by solar data straight from the time of printing while also affected by the biomaterials' hygroscopic properties. A specific case study was examined to embed environmental parameters of

specific geolocations into the workflow. This environmental and geographical contextualisation allowed to link biomaterial deposition with heat stress and understand how the material distribution of the multi-biomaterial lattice could be optimised to support biological growth in future. The inclusion of environmental data, material and fabrication parameters in the design stage, is potentially facilitating the creation of bio-integrated, multi-material prototypes that can lead the way to future animate architecture. The produced prototypes in this study were automated but not identical, creating resolution- and context-customised building components. This allows now to design and predict without predetermining the final outputs, enabling manufacturing to be in continuous negotiation with materials, the processes and the environment.

Declaration of competing interest

The authors declare that they have no known competing financial interests or personal relationships that could have appeared to influence the work reported in this paper.

Acknowledgements

The authors would like to thank Carlos Bausa Martinez and Konstantinos Zervos for their technical support and Prantar Tamuli and Ningkang Wen for their valuable feedback during the process. BP is affiliated with the UKRI Interdisciplinary Circular Economy Centre for Mineral-based Construction Materials (EP/V011820/1).

Appendix A. Supplementary data

Supplementary data to this article can be found online at https://doi.org/10.1016/j.foar.2022.06.010.

References

An, J., Teoh, J.E.M., Suntornnond, R., Chua, C.K., 2015. Design and 3D printing of scaffolds and tissues. Engineering 1 (2), 261—268.

Bae, K.H., Lee, F., Xu, K., Keng, C.T., Tan, S.Y., Tan, Y.J., Chen, Q., Kurisawa, M., 2015. Microstructured dextran hydrogels for burst-free sustained release of PEGylated protein drugs. Biomaterials 63, 146—157.

Ben Chekroun, K., Sánchez, E., Baghour, M., 2014. The role of algae in bioremediation of organic pollutants. Int. Res. J. Publ. Environ. Health 1 (2), 19—32.

Carpo, M., 2016. Excessive resolution: from digital streamlining to computational complexity. In: Campo, M. (Ed.), Evoking through Design: Contemporary Moods in Architecture. John Wiley & Sons, Oxford, pp. 78—83.

CFD Product team, 2019. Autodesk CFD. Autodesk.

Chatterjee, S., Chi-leung Hui, P., 2018. Stimuli-responsive hydrogels: an interdisciplinary overview. In: Popa, L., Ghica, M.V., Dinu-Pirvu, C.E. (Eds.), Hydrogels - Smart Materials for Biomedical Applications.

Chua, C., Yeong, W., 2015. Bioprinting, Principles and Applications. World Scientific, New Jersey.

Duro-Royo, J., Mogas-Soldevila, L., Oxman, N., 2015. Flow-based fabrication: an integrated computational workflow for design and digital additive manufacturing of multifunctional heterogeneously structured objects. Comput. Aided Des. 69, 143—154.

Fondriest Environmental Inc, 2014. Solar Radiation & Photosynthetically Active Radiation - Environmental Measurement Systems. Available at: https://www.fondriest.com/environmental-measurements/parameters/weather/photosynthetically-active-radiation/.

Grigoriadis, K., 2018. The current state of autography. Int. J. Rapid Manuf. 7 (2/3), 277—294.

Groat, L., Wang, D., 2013. Architectural Research Methods, second ed. John Wiley & Sons.

Harding, J., Olsen, C., 2018. Biomorpher (0.7.0). MIT license.

Hensel, M., Menges, A., 2006. Nestled capacities. In: Lally, S., Young, J. (Eds.), Softspace. Routledge, London.

Hughes, R., 2019. CNC post. Available from: G-code for a CNC Mill - Grasshopper - McNeel Forum.

Kim, M.H., Lee, Y.W., Jung, W.K., Oh, J., Nam, S.Y., 2019. Enhanced rheological behaviors of alginate hydrogels with carrageenan for extrusion-based bioprinting. J. Mech. Behav. Biomed. Mater. 98, 187—194.

Kreysler, B., 2010. Craft in digital design. In: Lynn, G., Gage, M.F. (Eds.), Composites, Surfaces, and Software: High Performance Architecture. W. W. Norton, New York, pp. 37—53.

Li, J., Wu, C., Chu, P., Gelinsky, M., 2020. 3D printing of hydrogels: rational design strategies and emerging biomedical applications. Mater. Sci. Eng. Rep 140, 4—76.

Liu, Z., Bhandari, B., Prakash, S., Mantihal, S., Zhang, M., 2019. Linking rheology and printability of a multicomponent gel system of carrageenan-xanthan-starch in extrusion based additive manufacturing. Food Hydrocoll. 87, 413—424.

Malafouris, L., 2018. Mind and material engagement. Phenomenol. Cognitive Sci. 18 (1), 1—17.

Malik, S., Hagopian, J., Mohite, S., Lintong, C., Stoffels, L., Giannakopoulos, S., Beckett, R., & Leung, C., Ruiz, J., Cruz, M. & Parker, B. (2020). Robotic extrusion of algae-laden hydrogels for large-scale Applications. Global Challeng.. 4(1), 1-12..

[Proving ground] Miller, N., 2019. Introduction to LunchBoxML - Tutorial. Available from: https://www.youtube.com/watch?v=e6WglyUB-7A.

Miller, N., 2020. LunchBox for Grasshopper.

Min, L.J., Edgar, T.Y.S., Zicheng, Z., Yee, Y.W., 2015. Biomaterials for bioprinting. In: Zhang, L., Leong, K., Fisher, J. (Eds.), 3D Bioprinting and Nanotechnology in Tissue Engineering and Regenerative Medicine. Elsevier, pp. 129—148.

Mogas -Soldevila, L., Duro -Royo, J., Oxman, N., 2014. Water-based robotic fabrication: large-scale Additive manufacturing of functionally graded hydrogel composites via multichamber extrusion. 3D Print. Addit. Manuf. 1 (3), 141—151.

National Institute of Biomedical Imaging and Bioengineering (NIBIB), 2021. Biomaterials. Available from: https://www.nibib.nih.gov/science-education/science-topics/biomaterials.

Oxman, N., 2013. Towards a material ecology. In: ACADIA, *Proceedings of the 32nd Annual Conference of the Association for Computer Aided Design in Architecture*, pp. 19—20. San Fransisco.

Payne, A., Johnson, J.K., 2015. Firefly.

Peters, B., 2018. Defining environments: understanding architectural performance through modelling, simulation and visualisation. Architect. Des 88 (1), 82—91.

Peters, T., Peters, B., 2017. Computing the Environment: Digital Design Tools for Simulation and Visualisation of Sustainable Architecture. John Wiley & Sons, Hoboken, New Jersey.

Piker, D., 2017. Kangaroo.

Rutten, D., Robert McNeel and Associates, 2009. Grasshopper 3D.

Sayre, R., 2010. Microalgae: the potential for carbon capture. Bioscience 60 (9), 722—727.

Smith, R., Bader, C., Sharma, S., Kolb, D., Tang, T., Hosny, A., Moser, F., Weaver, J., Voigt, C., Oxman, N., 2019. Hybrid living materials: digital design and fabrication of 3D multimaterial

structures with programmable biohybrid surfaces. Adv. Funct. Mater. 30 (7), 1—14.

Tai, Y., Bader, C., Ling, A., Disset, J., Darweesh, B., Duro-Royo, J., Van Zak, J., Hogan, N., Oxman, N., 2018. Designing (for) decay: parametric material distribution for hierarchical dissociation of water-based biopolymer composites. In: Mueller, C., Adriaenssens, S. (Eds.), Creativity in Structural Design. International Association for Shell and Spatial Structures (IASS), Boston, pp. 1—8.

The Royal Society, 2021. Animate Materials. The Royal Society, London. Available from: https://royalsociety.org/-/media/policy/projects/animate-materials/animate-materials-report.pdf.

Tsou, Y.H., Khoneisser, J., Huang, P.C., Xu, X., 2016. Hydrogel as a bioactive material to regulate stem cell fate. Bioact. Mater. 1 (1), 39—55.

Tamuli, P., Salmane, A., Jotanovic, N., Cruz, M., Parker, B., 2021. Engineered Living Materials. UK Patent Application No. 2113331.9.

Wang, S., Lee, J., Yeong, W., 2015. Smart hydrogels for 3D bioprinting. Int. J. Bioprint. 1 (1), 3—14.

Wiscombe, T., 2012. Beyond assemblies: system convergence and multi-materiality. Bioinspiration Biomimetics 7 (1), 1—7.

W-LAB, 2021. W-LAB. Available from: W-LAB (wds-lab.com).

Zhu, X., Zhang, Y., Deng, J., Luo, X., 2018. Effect of glycerol on the properties of the cross-linked polyvinyl alcohol hydrogel beads. ChemistrySelect 3 (2), 467—470.